Published in final edited form as:
*Opt Express*. 2008 December 22; 16(26): 21434–21445.

# Remote plethysmographic imaging using ambient light

**Wim Verkruysse**[1,*], **Lars O Svaasand**[2], and **J Stuart Nelson**[1]

[1]Beckman Laser Institue, University of California, Irvine, 1002 Health Sciences Rd. East, Irvine, CA. 92612, USA

[2]Faculty of information technology, mathematics and electrical engineering. Norwegian university of science and technology, Trondheim, Norway.

## Abstract

Plethysmographic signals were measured remotely (> 1m) using ambient light and a simple consumer level digital camera in movie mode. Heart and respiration rates could be quantified up to several harmonics. Although the green channel featuring the strongest plethysmographic signal, corresponding to an absorption peak by (oxy-) hemoglobin, the red and blue channels also contained plethysmographic information. The results show that ambient light photo-plethysmography may be useful for medical purposes such as characterization of vascular skin lesions (*e.g.*, port wine stains) and remote sensing of vital signs (*e.g.*, heart and respiration rates) for triage or sports purposes.

## 1. Introduction

Detection of the cardio-vascular pulse wave traveling through the body is referred to as Plethysmography ('Plethysmos' = increase in Greek) and can be done by means such as variations in air pressure, impedance, or strain. Photo-plethysmography (PPG), introduced in the 1930's [1] uses light reflectance or transmission and is the least expensive method and simple to use. PPG is based on the principle that blood absorbs light more than surrounding tissue so variations in blood volume affect transmission or reflectance correspondingly. Applications of PPG include monitoring of oxygen saturation (pulse oxymetry), heart (HR) and respiration (RR) rates, blood pressure, cardiac output, assessment of autonomic functions and detection of peripheral vascular diseases. Remote, non-contact pulse oxymetry and PPG imaging have been explored only relatively recently [2,3].

To our knowledge, PPG has always been performed with dedicated light sources and typically red and/or infra-red (IR) wavelengths. Due to the historical emphasis of PPG on pulse oxymetry and the associated need to sample relatively deep (*e.g.*, 1 mm) veins and arteries, the visible spectrum (with a shallower penetration depth in skin) has often been ignored as a light source for PPG. Publications describing non-red visible light sources for PPG (*e.g.* green) are either recent [4,5] or relatively old [6,7], and, in all cases, contact probes were used. Ambient visible light is often considered a source of noise [8–11] when using IR light sources and detectors sensitive for IR and visible light.

In this communication, we show that PPG signals can be remotely (several m) measured on the human face with normal ambient light as the source and a simple digital, consumer level photo camera in movie mode. At distances of 1.5 m, signal to noise ratio (SNR) was such that



*Corresponding author: E-mail: wverkruy@uci.edu.

**OCIS codes:** (280.4991) Passive remote sensing; (170.3880) Medical and biological imaging

up to four harmonics of the fundamental HR frequency can be measured, thus rendering not only the HR but also the shape of the waveform. In addition to HR and RR monitoring, we show that PPG imaging can be used to characterize regions of high and low pulsatility on facial port wine stains (PWS). PWS are cutaneous capillary malformations characterized by a higher number and/or a larger size of the pathologic capillaries [12]. A better understanding of the hemodynamics involved in PWS is of great interest to improve laser therapeutic outcome.

Our PPG results suggest that not only pulsatility but also phase information regarding the cardio-vascular waveform may be deduced. Although we will attempt to interpret clinical results and discuss their relevance, the main purpose of this paper is to demonstrate remote PPG (imaging) with ambient light. To the best of our knowledge, remote PPG (imaging) with ambient light has never been demonstrated.

## 2. Methods

### 2.1 Materials and set-up

Simple, inexpensive (< $200) digital cameras were used (Canon Powershot models A560, A570 and A640). Early measurements were taken with the A640 and A670 but later we preferred to use the A560 because the auto brightness function can be disabled (see discussion). After setting the camera in movie mode volunteers were asked to sit, stand or lie down to minimize any movements. With the camera on a tri-pod, movies were recorded of the facial area. Duration varied from 30 s to several minutes. Typically, daylight was used as the illumination source in combination with normal artificial fluorescent light. In a few cases, movies were taken of a port wine stain (PWS) patient, immediately before or after laser therapy in the operating room (OR) at the Beckman Laser Institute and Medical Clinic, (BLIMC, UC Irvine, CA). Here, the illumination was provided by a surgical lamp at the same light intensity used for surgery. No additional illumination was used in any of the data presented herein. Typically, the distance between camera and object was 1–2 m and no lens, other than the built-in 3× zoom, was used.

### 2.2 Spatial averaging to improve SNR

Color movies, recorded at either 15 or 30 frames per second (fps) and pixel resolution of 640×480 or 320×240, were saved in AVI format by the camera and transferred to a PC. Using Matlab®, (Mathworks) software, pixel values (PV, 8bit, 0–255) for the red (R), green (G) and blue (B) channels were read for each movie frame providing a set of PV($x$,$y$,$t$) where $x$ and $y$ are horizontal and vertical positions, respectively, and $t$ is time corresponding to the frame rate. Using a graphic user interface, regions of interest (ROI) were selected in a still (selected from the movie) and the raw signal ($PV_{raw}(t)$) was calculated as the average of all pixel values in the ROI.

For mapping purposes, we projected each movie frame on a coarse grid (50×40 cells) and, as with a ROI, calculated the average PV for each cell and frame. While compromising spatial resolution, such spatial averaging of the PV's was found to improve significantly SNR. After Fourier transforming PV(t), displaying the power at frequencies of interest (such as the HR) in each grid cell provides 'power maps'. Similarly, a phase (per frequency) was computed for each grid cell providing 'phase maps'. The coarse grid was also used to produce false color movies with pixel values PV($x$,$y$,t) where x and y now refer to the pixel position in the coarse grid and PV($x$,$y$,$t$) is filtered over time (see next section).

### 2.3 Digital filtering and spectral analysis (time domain)

Each of the PV($t$) signals, from a ROI or a pixel in the coarse grid, is presented in one of the following ways in this paper:

| | |
|---|---|
| $PV_{raw}(t)$ | no processing other than spatial averaging over ROI or coarse grid cell; |
| $PV_{AC}(t)$ | the mean over time of $PV_{raw}(t)$ is subtracted (= $PV_{raw}(t)$ minus DC); or |
| $PV_{BP}(t)$ | band-pass filtered $PV_{raw}(t)$ signal. |

For the band-pass (BP) filter Butterworth coefficients ($4^{th}$ order) were used in a phase neutral (forward and reverse) digital filter ("filtfilt" in Matlab®). Cut-off frequencies for the BP filter will be listed in the results section.

Fast Fourier transforms ("FFT" in Matlab®) on PV($t$) signals were performed to determine the power and phase spectra for PV($t$). Zero padding of PV($t$) prior to the Fourier transform was used to allow for a finer discretization of the frequency. We will refer to an $n^{th}$ order zero padding if the original signal was expanded on both sides with a 0 signal of length n times the original time span.

Plethysmographic signals are sometimes presented inverted to render the intensity proportional to blood pressure or volume. In this communication, all signals will be presented directly: a higher signal corresponds to a higher reflectance and smaller blood volume. Although we will indicate how pixel values (the basic measurement unit) relate to reflectance, all signals will be presented in pixel values.

## 3 Results

### 3.1 HR and RR detection

Figure 1 shows $PV_{raw}(t)$ signals for the G and B channels (R not shown), extracted from a 290 s movie of a volunteer who was asked to perform 50 knee bends. Five seconds after the exercise ended, the volunteer sat on a chair and was asked to hold his/her unsupported head still. The ROI for which signals are shown is a rectangular area on the forehead (ROI I in Fig. 2(a)). Dips in $PV_{raw}(t)$ (*e.g.*, around $t = 35$ s and $t = 90$ s) are likely due to involuntary movements, changing the angle of the forehead slightly, resulting in a lower signal. DC levels or low frequencies (< 0.1 Hz) are typically not considered in PPG due to the fact that calibration of such signals is difficult [13]. In our approach, using ambient light and a camera which applies several automatic brightness and color functions on each channel, calibration is an even more difficult task. Herein, we will not address the DC and low frequency variations and instead focus on the AC signals.

The plethysmographic information is visible in the Fig. 1(a) inserts. Oscillations for HR and RR are indicated in the G and B channels, respectively (left insert). The HR is better visible in Figs. 1(b) and (c), displaying the joint time-frequency diagrams of the signals (G and B, respectively) in Fig. 1(a) for a time window of 10 s (300 frames). The HR gradually decreases from $t = 0$ to 100 s, as the volunteer recuperates from the physical exercise. The HR and RR signals are most pronounced in the G and B channels, respectively, and both decrease gradually during recuperation. The fundamental HR frequency and, even the $2^{nd}$ through $4^{th}$ harmonics, can be identified in Fig. 1(b). Detection of the harmonics indicates that both the HR but and the shape of the plethysmogram were determined.

At $t = 180$ s the volunteer appeared to be fully recuperated and was asked to in- and exhale deeply and, at a more rapid pace, until $t = 230$ s whereupon the volunteer was asked to breath normally. During this voluntary hyperventilation RR increases in frequency and amplitude (Fig. 1(c)). Simultaneously, HR gradually increases from 1.1 to 1.5 Hz at $t$ =215 s after which it gradually decreases. HR peaks *before* hyperventilation stopped, indicating that HR is

autonomically controlled and measured independent of RR. The observed RR and HR evolutions are consistent with the literature [14].

Quantification of HR, both at rest and after physical exercise, was found to be in excellent agreement with HR quantified by a commercial pressure cuff with a digital HR display. We are aware, however, that HR related signals could also be introduced through movements of the head. Any slight movement could move a relatively dark area in and out of the ROI with a periodicity equal to the HR and would also appear as plethysmographic signals. Such signals, however, would be fundamentally different from what is normally referred to as PPG: a signal induced by temporal variation in blood volume and corresponding variations in light absorption. Comparison of $PV_{AC}(t)$ signals are shown in Fig. 2(a) for three additional ROI's (II – IV), indicated in Fig. 2(b), provides evidence that the signals in Fig. 1 are true PPG signals. If HR related movements combined with contrast variations were due to the strong HR signal shown in Fig. 1 at 1.1 Hz, a smaller ROI than I should provide an even stronger HR signal since the many pixels in the bulk of ROI I, do not contribute to the HR signal (only contrast variations at the edges of ROI I would contribute). However, even a single pixel (ROI II) has the same power at the HR as ROI I (Fig. 2(c)). The main difference is that the signal for ROI II contains more noise as compared to than that for ROI I. Apparently, each pixel in ROI contributes to the HR signal while camera noise (per pixel) is reduced by averaging leading to a much higher SNR than for a single pixel. The $PV_{AC}(t)$ signal for ROI III is strong due to the high contrast combined with involuntary movements. However, the power spectrum (Fig. 2 (c)) does not indicate that movements are predominant at HR: the spectrum basically indicates noise, associated with movements at random frequencies. Both comparisons are consistent with the hypothesis that the signals in Fig. 1 are true PPG signals. Finally, the fact that the G channel almost always features a much stronger HR signal as compared to the R and B channels, is also strong evidence that the signals are filtered by variations in blood volume (due to the absorption bands for oxy-and de-oxy hemoglobin for yellow and green light).

ROI IV, encompassing the entire face, illustrates that selection of the ROI is not critical for the HR determination. The amplitude of the HR signal is reduced (due to the inclusion of many background pixels) but the noise is also reduced, leaving the SNR intact: even the 3$^{rd}$ harmonic is well above camera noise level (Fig. 2(c)). Movement artifacts combined with stark contrasts such as the eyes, nose, mouth or face compared to image background PV's cancel out in the signal for ROI IV. The RR can be clearly identified at 0.27 Hz. The noise level as a function of frequency in Fig. 2(c) (IV) is consistent with 1/frequency noise (not shown), which is characteristic for CCD detectors.

### 3.2 Modulation of RR and HR

Whereas Fig. 1 – Fig. 2 show the RR and HR as baseline modulated signals (DC modulation), an example of pulse amplitude modulation (AC modulation) is shown in Fig. 3. Data was extracted from a movie (shown in the left panel in media 1) recorded at 30 fps and 320×240 pixel resolution. Figs. 3(b) and (c) are $PV_{AC}(t)$ and $PV_{BP}(t)$ maps, respectively, for $t = 6$ s. The display (false color) amplitude for Fig. 3(c) is 5× that of Fig. 3(b) to compensate for the much lower HR amplitude. The full $PV_{AC}(t)$ and $PV_{BP}(t)$ signals (30 s) are shown in Figs. 3(d) and (f) where dashed vertical lines indicate the time for Figs. 3(a–c). The power spectrum for the G channel is shown in Fig. 3(e). The strongest signal at 0.12 Hz represents RR (harmonics are indicated) while 3 peaks in the HR frequency range (1, 1.12 and 1.24 Hz) are consistent with an amplitude modulation of HR at 1.12 Hz with RR at 0.12 Hz. Fig. 3(f) shows $PV_{BP}(t)$ (0.8 – 6 Hz) also illustrating the ampltidue modulation of RR and HR.

The amplitude relationship between R, G and B channels shown in Fig. 3(f) is typical for most data we have obtained so far: the strongest plethysmographic signal is for the G channel, although the RR signal is sometimes more pronounced in the R or B channel (as in Fig. 1(c)).

Note that the RR signals in Fig. 3d for the three channels are different in shape as well as amplitude, suggesting that they may contain complementary information regarding oxygenation or depth origin of the pulsation (red light penetrates deeper in human skin as compared to blue). The RR induced R and B channel signals are well above the noise level and are lower than the G channel signal possibly due to a low absorption coefficient by blood for the R channel [15] and a small probing volume for the B channel. The HR signals for the R and B channels in Fig 3(f) are close to the noise level.

### 3.3 Pulse amplitude mapping

As discussed in section 3.1 and illustrated by the signal for ROI III in Fig. 2, movement artifacts are likely not HR related, however, they are still important when generating pulsatility (power) maps. Areas with high contrast moving in and out of the ROI will feature strong fluctuations and, thus, correspond to increased powers for a large range of frequencies, including the HR (*e.g.*, see the power spectrum for ROI III in Fig. 2(c),).

A simple method to reduce such artifacts in power maps is illustrated in Fig. 4. Comparing the G channel of a movie frame and the corresponding power map (Figs. 4(a–b)) for the movie at the HR of this volunteer (1.06 Hz, power map is for a 23 s signal at 30 fps) shows relatively high powers in areas with high contrast. Under the assumption that movement artifacts mostly induce 'white noise' (no dominant frequency) around the HR frequency (as is plausible from the power spectrum for ROI III, Fig. 2(c)), we determine a 'movement artifact map' by averaging the powers at bandwidths around the HR. Such a map, (Fig. 4(c)) indicates that areas with high contrast (Fig. 4(a)) are indeed associated with high powers. After subtracting the movement artifact map from that in 4b, we obtain the map corrected for movement artifacts (Fig. 4(d). A range of better artifact reductions could be applied such as software to laterally synchronize the movie frame by frame. Such software is currently unavailable, however, and we used the described correction method as a preliminary attempt. All power maps shown herein are corrected in this way.

A critical look at the power map in Fig. 4(d) in comparison with the image in 4(a) suggests that the pulse power map correlates with the intensity of the G channel. Lighter areas in 4(a) often feature a higher pulse signal in 4(b), and *vice versa*. Until we have established better ways to deal with shading (due to facial curvature etc.) the presented power maps should not be interpreted as robust maps of relative pulsatilities. Nevertheless, in pulse amplitude maps of several PWS patients, we have often observed clear pulsatility contrasts between normal and adjacent PWS skin indicating the feasibility of plethysmographic imaging. In normal skin HR pulse amplitudes (G channel) were typically 2 – 4 times higher than in adjacent PWS skin: *e.g.* 0.75 and 0.25 PV, respectively.

From calibration experiments (unpublished) we have determined that the pixel values of the used digital cameras can be related to light intensities as $Y \approx 73 \ln(I) + k$, where Y is a channel (R, G or B) pixel value, I is the actual light intensity to which a CCD pixel is exposed and k is a constant which depends on camera parameters such as exposure time and aperture. Using this relationship we estimate the variation in reflectance during a heart beat cycle from the amplitude of the HR plethysmograms (in PV). For example, a HR pulse amplitude of 0.75 PV corresponds to a 1% variation in reflectance (*e.g.* from 20 to 20.2% reflectance [16,17] for green/yellow light).

### 3.4 Phase mapping

An example of mapping phase differences using plethysmographic imaging is shown in Fig. 5 and a movie (media 2). Figure 5(a) shows a still from a PWS patient who underwent laser therapy 5 minutes prior to the movie recording. Media 2 shows the $PV_{BP}(t)$ movie (BP filter:

0.8 – 6 Hz., G channel) of which excerpts (frames 9 and 22) are shown in Figs. 5(b) and (c). In Fig. 5b the PWS area has a higher intensity as compared to surrounding normal skin (note, this is true for the AC signal, the DC intensity is still lower) and Fig. 5(b) shows that 0.43 s later, the opposite is true. A phase map for the HR frequency of 1.43 Hz is shown in Fig. 5d. The approximate phases of the frames in Fig. 5(b,c) are indicated by the circle and triangle in Figs. 5(e,f). The Lissajous presentation (Fig. 5(f)) shows that the phase difference persists during the full 33 s. (43 heart beat cycles) of the movie recording. The Lissajous curve for the PWS signal shifted by 2 frames (Fig. 5(g)) shows that the phase difference can be quantified as approximately 0.067 s, or 34 degrees at a HR of 1.43 Hz.

Some areas in Fig. 5(h) can be identified as distinctly lower pulsatility (arrows) and correspond to areas that show some purpura (discoloration) due to laser therapy. Interestingly, they seem to be surrounded by areas with relatively higher pulsatility. The strong contrast between PWS and normal skin in the phase map (Fig. 5(d)) is remarkable, in particular when compared to the relative lack of contrast in the power map. To our knowledge such a phase difference in PWS has never been reported nor discussed in literature. We have not yet been able to explain these intriguing hemodynamic phenomena.

### 3.5 Cardio-vascular wave propagation

To illustrate interesting spatio-temporal features of the PPG signals and contrast between pulsatility in PWS and adjacent normal skin plethysmographic images are shown in Fig. 6 and media 3. The panels in Media 3 are (from left to right) $PV_{BP}(t)$ maps (BP filter: 0.8 – 2 Hz) for the R, G and B channels and the actual movie (reduced resolution), respectively. A movie excerpt from media 3 ($t$ = 3.4 s, frame 103) is shown in Figs. 6(a–d). In the carotid artery area (neck to ear), the $PV_{BP}$ movies for each of the channels often appear to show an upward direction of relative intensity. We tentatively interpret this as the cardio-vascular wave. Although for most heart beats the periodic intensity variation is spread out laterally and lacks a clear definition of vascular structure, the arrow in Fig. 6(b) indicates a structure which may indeed be the carotid artery. The power maps for the full 30 s movie (Figs. 6(e–g)) average out the seemingly random lateral dispersion of the wave and show a similar longitudinal structure as indicated in Fig 6(b). This structure is best defined in the power map for the R channel (Fig. 6(e), arrow).

The phase map for the G channel (Fig. 6(h)) shows a small but distinct gradient (arrow) which corresponds to the general upward direction of the wave propagation displayed in Media 3. Although the carotid artery, presumably imaged in Figs. 6(e,f), is not visible on the phase map, a phase contrast between the general carotid artery area and the rest of the imaged face can be seen.

In all three power maps (Figs. 6(e–g)) the relatively high powers in the lower right corner (arrows in Figs. 6(f,g)) are movement artifacts. In the original, non compressed movie, this area can be clearly seen to pulsate as the cardio-vascular waves propagate through the carotid artery. Even the adjacent hair moves synchronously. Since these displacements are clearly dominated by the HR, the described correction method (section 3.3) fails to remove these artifacts. Given the strong physical displacement of skin by the left carotid artery, we are aware that the relatively strong signals in the patient's right carotid artery area may also be (partly) due to displacements. A slight displacement may easily modify the illumination (angle) of this area, synchronously with the HR. For a further discussion regarding the interpretation of these results see below.

# 4 Discussion

## 4.1 General

We have shown that movies of the human face, recorded with a simple digital camera and ambient light as the only source of illumination, contain robust reflectance PPG signals. Typically the G channel contains the strongest plethysmographic signal, consistent with the fact that (oxy-) hemoglobin absorbs green light better than red [15] and penetrates sufficiently deeper into the skin as compared to blue light to probe the vasculature. However, it should be noted that the R and B channels may contain complementary information (Fig. 3(d)). RR, HR, and their mutual modulation, can be determined (Fig. 1–Fig. 3). Often, harmonics of the RR and HR are above the noise level which provides information regarding the shape of the plethysmograms. Lateral variations in pulsatility and phase of the cardio-vascular wave have been demonstrated in PWS (Fig. 5 and Fig. 6). With the expressed reservation, we believe that the carotid artery may have been imaged in one volunteer (Fig. 6(e)).

Two main issues limit the spatial resolution of the PPG images (power and phase) and accuracy of our current approach. First, movement artifacts and, second, reduced SNR due to CCD generated noise in the recorded pixel values. The first issue may be solvable by improved positioning of the volunteers (often the subjects were standing or sitting without head support), software to laterally synchronize frames and more homogeneous (artificial) illumination to reduce shading artifacts. The second issue may be abetted by simply using more advanced movie cameras with higher pixel resolution, allowing for a good SNR through pixel averaging while maintaining a good spatial resolution in the PPG images.

## 4.2 Artifacts

Although concerns regarding artifacts have been addressed in the results section, some require additional discussion. The movie of $PV_{AC}(t)$ (central panel in media 1) shows that the respiration signal of the cheek is out of phase with the rest of the face (*e.g.*, compare frames for $t = 7$ and 10s). It is possible that the cheek area is slightly displaced during respiration, and, thus, modulating illumination. The overall RR signal, however, is most likely not artifactual. The RR signal for the three channels have different shapes (Fig. 3(d)) which is inconsistent with illumination/displacement artifacts. Moreover, the clear AC modulation of RR and HR also indicates that the overall RR signal is a true PPG signal. Shading has been acknowledged as a problem in PPG imaging and is being tackled by advanced technology [18]. Obviously, our PPG imaging approach has yet to date not advanced to these dev elopmental stages.

A similar displacement artifact (now HR related) may underlie at least part of the strong signals in the right carotid artery area shown in Fig. 6. The fact that all three channels (R,G and B) feature a high power in Figs. 6(e–g) is consistent with this hypothesis. On the other hand, they do show *some* differential features. In particular, the map for the R channel, (a wavelength band closer to the wavelengths used for PPG imaging [2]) appears to indicate a vessel like structure, exactly where the carotid artery is embedded. Even if some of the features in Fig. 6 are displacement artifacts it should be noted that they are basically true plethysmographic signals (measuring volume changes). In fact, tissue pulsatility measured with ultrasound [19] is plethysmography as well. However, the observed features may be not pure PPG as it is commonly understood.

A last source of potential artifacts is that the camera models A570 and A640 have automatic functions to adjust gain during movie recording. Such automatic adjustments decrease the dynamics of the plethysmographic signals (gain goes up when the subject becomes darker and *vice versa*). Therefore, it is possible that the signal amplitudes are in fact higher than those measured with these cameras. More worrisome, however, is the fact that the auto-gain functions

have a time constant (the adjustment is gradual) and that it is not constant for the entire CCD chip but depends on the local light intensity. If, therefore, the time constant for the auto-gain is different for a PWS area (darker) as compared to normal skin, a phase delay could be induced. Concerned that the HR signal phase differences pointed out in Fig. 5 are related to this, we tested the A640 for such artifactual phase delays. Animated computer graphics were made to simulate a PWS and adjacent normal skin area (comparable color and pulsatility as in real movies of PWS patients) and recorded with the A640. Phase analysis in a similar way as presented for real PWS herein showed no sign whatsoever that phase changes could be artifactually induced. The A560 model has an option to switch off the auto-gain function which, therefore, is our preferred camera until we locate better cameras for our purpose.

### 4.3 Remote sensing

All herein presented plethysmographic signals were recorded without additional optical lenses other than the built-in 3× zoom. Since there is interest in remote sensing of HR for combat triage [20] or for athletic monitoring purposes, we tried briefly to use a tele-lens (2×) in combination with one of our digital cameras. At a distance of 11 m between the camera and subject, the signal contained more noise than the signals in Fig. 1 but the fundamental HR frequency could still be identified very clearly for relatively short time windows of 10s. Using movie camera's with stronger optical zoom options and higher pixel definitions, we expect to measure HR (and possibly RR) at greater distances than 11 m. This will be the subject of a future study.

### 4.4 Future directions

The strong signals in visible light are surprising in the sense that PPG plethysmography has been practiced for many decades while we found few studies exploiting this band, despite explicit recommendations by Crowe *et al.* [7] to use green/yellow light for which hemoglobin has absorption peaks [15] (consistent with our finding that the G channel has the strongest plethysmographic signals). This is perhaps due to the strong relationship between plethysmography and pulse oximetry. The latter has traditionally used red and IR wavelengths, one of which is at an isobestic point for oxy- and de-oxyhemoglobin. Although for pulse oximetry these wavelengths are probably the right choice, the demonstrated method has distinct opportunities in other applications. As Gailite [4], Jonsson [21] and Lindberg [6] pointed out, reduction of the sampling depth using shorter wavelengths has advantages if superficial microvasculature rather than deeper vasculature is the focus of PPG. In our research to understand PWS and its response to laser therapy, this is indeed the case. We plan to use spectrally resolved reflectance models [16,17,22] and hemodynamic models [23,24] to understand the measured PPG signals' relationship to PWS laser therapeutic outcome. Obviously, a more systematic categorization of PPG in PWS compared to adjacent skin as well as relative phase differences needs to be done. Currently, while improving the experimental conditions, we are in the process of designing such a study. Potentially this will reveal useful information, complementary to existing, but relatively complex methods to characterize hemodynamics of PWS such as laser speckle imaging [25], laser Doppler imaging [26] and Doppler optical coherence tomography [27]. In particular the relative phase differences (Fig. 6) and the differential plethysmogram shapes for PWS and normal skin are intriguing and show promise to help understand PWS hemodynamics beyond their current level.

All of the results in this manuscript concern measurements on the human face. Although we have measured clear PPG signals on other anatomical locations (*e.g.*, wrist, leg) the facial signals were typically stronger, the forehead in particular. For the application of remote detection of vital signals for triage and sports this is helpful because the face is usually uncovered. A robust comparison of PPG signal strengths as a function of anatomical location is a subject for future investigation.

## Acknowledgment

This work was made possible through the following NIH funds: AR47551 and EB2495.

## References and links

1. Hertzman AB, Spealman CR. Observations on the finger volume pulse recorded photoelectrically. Am. J. Physiol 1937;119:334–335.
2. Wieringa FP, Mastik F, van der Steen AFW. Contactless multiple wavelength photoplethysmographic imaging: A first step toward "SpO(2) camera" technology. Ann. Biomed. Eng 2005;33:1034–1041. [PubMed: 16133912]
3. Hu, S.; Zheng, J.; Chouliaras, V.; Summers, R. Feasibility of imaging photoplethysmography; Proceedings of the International Conference on BioMedical Engineering and Informatics; NewYork: Institute of Electrical and Electronics Engineers; 2008. p. 72-75.
4. Gailite L, Spigulis J, Lihachev A. Multilaser photoplethysmography technique. Lasers Med. Sci 2008;23:189–193. [PubMed: 17632746]
5. Jonsson, A. PhD thesis. Mälardalen University Press; 2006. Pressure Sore Etiology - Highlighted with Optical Measurements of the Blood Flow,Chapter 3, New sensor design made to discriminate between tissue blood flow at different tissue depths at the sacral area.
6. Lindberg LG, Oberg PA. Photoplethysmography II. Influence of light-source wavelength. Med. Biol. Eng. Comput 1991;29:48–54. [PubMed: 2016920]
7. Crowe, JA.; Damianou, D. The Wavelength Dependence of the Photoplethysmogram and its implication to Pulse Oximetry; Proceedings of the Annual International Conference of the IEEE Engineering in Medicine and Biology Society; NewYork: Institute of Electrical and Electronics Engineers; 1992. p. 2423-2424.
8. Cheang, PY.; Smith, PR. An Overview of Non-contact Photoplethysmography. LE11 3TU, UK: Department of Electronic and Electrical Engineering, Loughborough University; 2003. retrieved August 27, 2008, http://www.lboro.ac.uk/departments/el/research/esc-miniconference/papers/cheang.pdf.
9. Pollard JA. Cardiac arrhythmias and pulse variability. A plethysmographic study. Anaesthesia 1970;25:63–72. [PubMed: 5413231]
10. Hummler HD, Engelmann A, Pohlandt F, Högel J, Franz AR. Accuracy of pulse oximetry readings in an animal model of low perfusion caused by emerging pneumonia and sepsis. Intensive. Care. Med 2004;30:709–713. [PubMed: 14722632]
11. Trivedi NS, Ghouri AF, Shah NK, Lai E, Barker SJ. Effects of motion, ambient light, and hypoperfusion on pulse oximeter function. J. Clin. Anesth 1997;9:179–183. [PubMed: 9172022]
12. Barsky SH, Rosen S, Geer DE, Noe JM. The nature and evolution of port wine stains: A computer-assisted study. J. Invest. Dermatol 1980;74:154–157. [PubMed: 7359006]
13. Allen J. Photoplethysmography and its application in clinical physiological measurement. Physiol. Meas 2007;28:R1–R39. [PubMed: 17322588]
14. Ford MJ, Camilleri MJ, Hanson RB, Wiste JA, Joyner MJ. Hyperventilation, central autonomic control, and colonic tone in humans. Gut 1995;37:499–504. [PubMed: 7489935]
15. van Kampen, E.; Zijlstra, W. Determination of hemoglobin and its derivatives. In: Sobotka, H.; Stewart, C., editors. Advances in Clinical Chemistry. New York: Academic Press; 1965. p. 158
16. Verkruysse W, Lucassen GW, van Gemert MJC. Simulation of color of port wine stain skin and its dependence on skin variables. Lasers Surg. Med 1999;25:131–139. [PubMed: 10455219]
17. Svaasand LO, Norvang LT, Fiskerstrand EJ, Stopps EKS, Berns MW, Nelson JS. Tissue parameters determining the visual appearance of normal skin and port-wine stains. Lasers Med. Sci 1995;10:55–65.
18. Wieringa FP, Mastik F, ten Cate FJ, Neumann HAM, van der Steen AFW. Remote non-invasive stereoscopic imaging of blood vessels: First in-vivo results of a new multispectral contrast enhancement technology. Ann. Biomed. Eng 2006;34:1870–1878. [PubMed: 17048103]

19. Kucewicz JC, Dunmire B, Giardino ND, Leotta DF, Paun M, Dager SR, Beach KW. Tissue pulsatility imaging of cerebral vasoreactivity during hyperventilation. Ultrasound Med. Biol 2008;34:1200–1208. [PubMed: 18336991]

20. Wendelken, S.; McGrath, S.; Blike, G.; Akay, M. The feasibility of using a forehead reflectance pulse oximeter for automated remote triage; Bioengineering Conference, 2004. Proceedings of the IEEE 30th Annual Northeast; 2004. p. 180-181.

21. Jonsson, A. "New sensor design made to discriminate between tissue blood flow at different tissue depths at the sacral area," report #1098. Mälardalen Research and Technology Centre; 2006.

22. Verkruysse W, Lucassen GW, de Boer JF, Smithies DJ, Nelson JS, van Gemert MJC. Modelling light distributions of homogeneous versus discrete absorbers in light irradiated turbid media. Phys. Med. Biol 1997;42:51–65. [PubMed: 9015808]

23. Gross JF, Intaglietta M, Zweifach BW. Network model of pulsatile hemodynamics in the microcirculation of the rabbit omentum. Am. J. Physiol 1974;226:1117–1123. [PubMed: 4824864]

24. Huo YL, Kassab GS. Pulsatile blood flow in the entire coronary arterial tree: theory and experiment. Am. J. Phys.-Heart Circul. Phys 2006;291:H1074–H1087.

25. Huang YC, Ringold TL, Nelson JS, Choi B. Noninvasive blood flow imaging for real-time feedback during laser therapy of port wine stain birthmarks. Lasers Surg. Med 2008;40:167–173. [PubMed: 18366081]

26. Forrester KR, Stewart C, Tulip J, Leonard C, Bray RC. Comparison of laser speckle and laser Doppler perfusion imaging: measurement in human skin and rabbit articular tissue. Med. Biol. Eng. Comput 2002;40:687–697. [PubMed: 12507319]

27. Nelson JS, Kelly KM, Zhao YH, Chen Z. Imaging blood flow in human port-wine stain in situ and in real time using optical Doppler tomography. Arch. Dermatol 2001;137:741–744. [PubMed: 11405763]

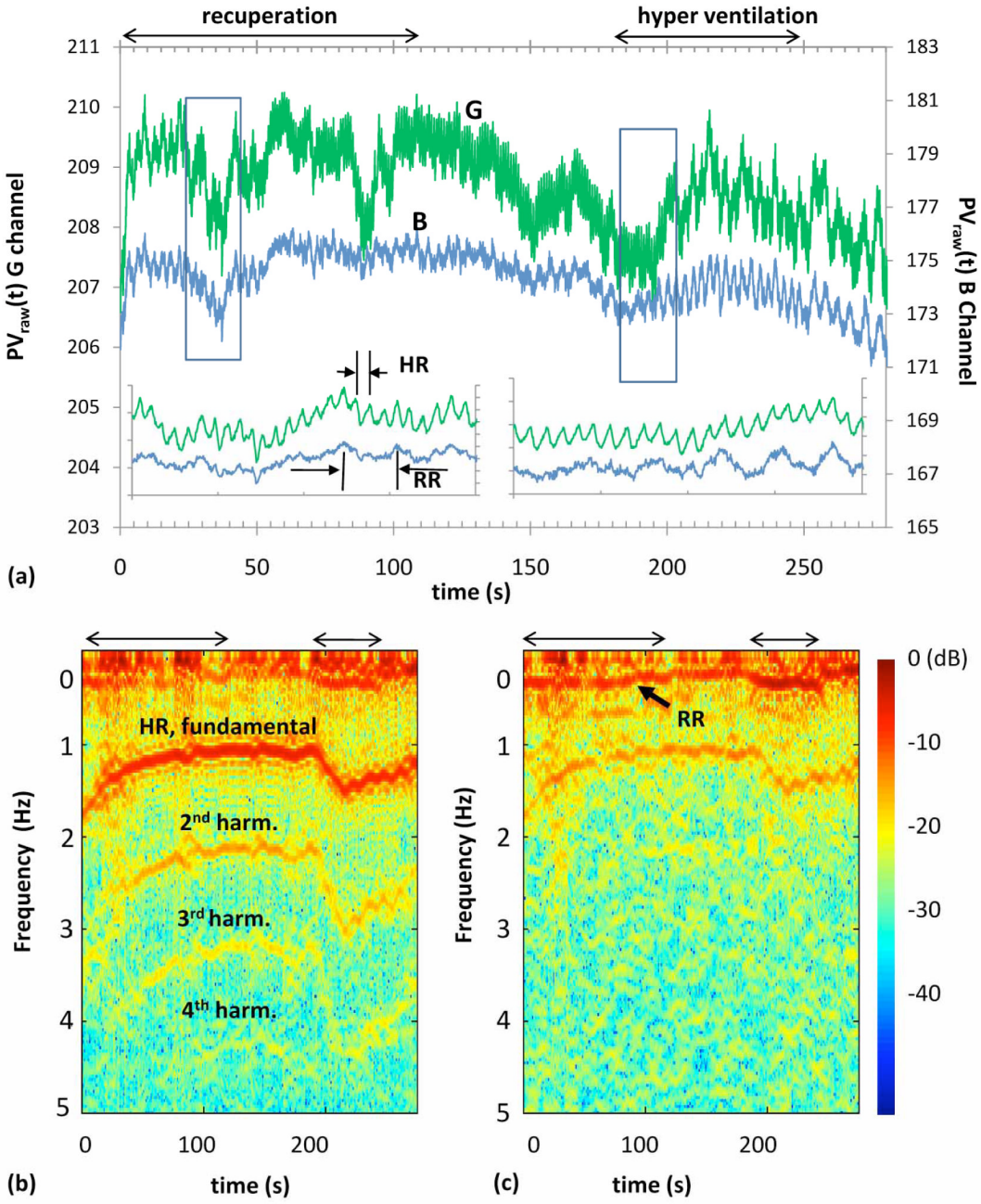


**Fig. 1.**

(a): $PV_{raw}(t)$ signals for G and B channels as indicated and a ROI on the forehead (ROI I in Fig. 2(b)). Movie recording started 5 s after the subject finished physical exercise. Boxed areas in (a) are shown as insert graphs. In the left insert ($t$ = 30–50s), HR can be observed to decrease. Impact of voluntary hyperventilation on RR and HR is best seen in the right ($t$ = 185 – 205 s). (b) and (c) Joint time-frequency diagrams (10 s time window) for G and B channels, respectively. HR decreases from 1.7 to 1.1 Hz during recuperation from $t$ = 0 – 120 s. In (c), the band associated with RR initially decreases gradually during recuperation and abruptly increases to 0.3 Hz during hyperventilation.

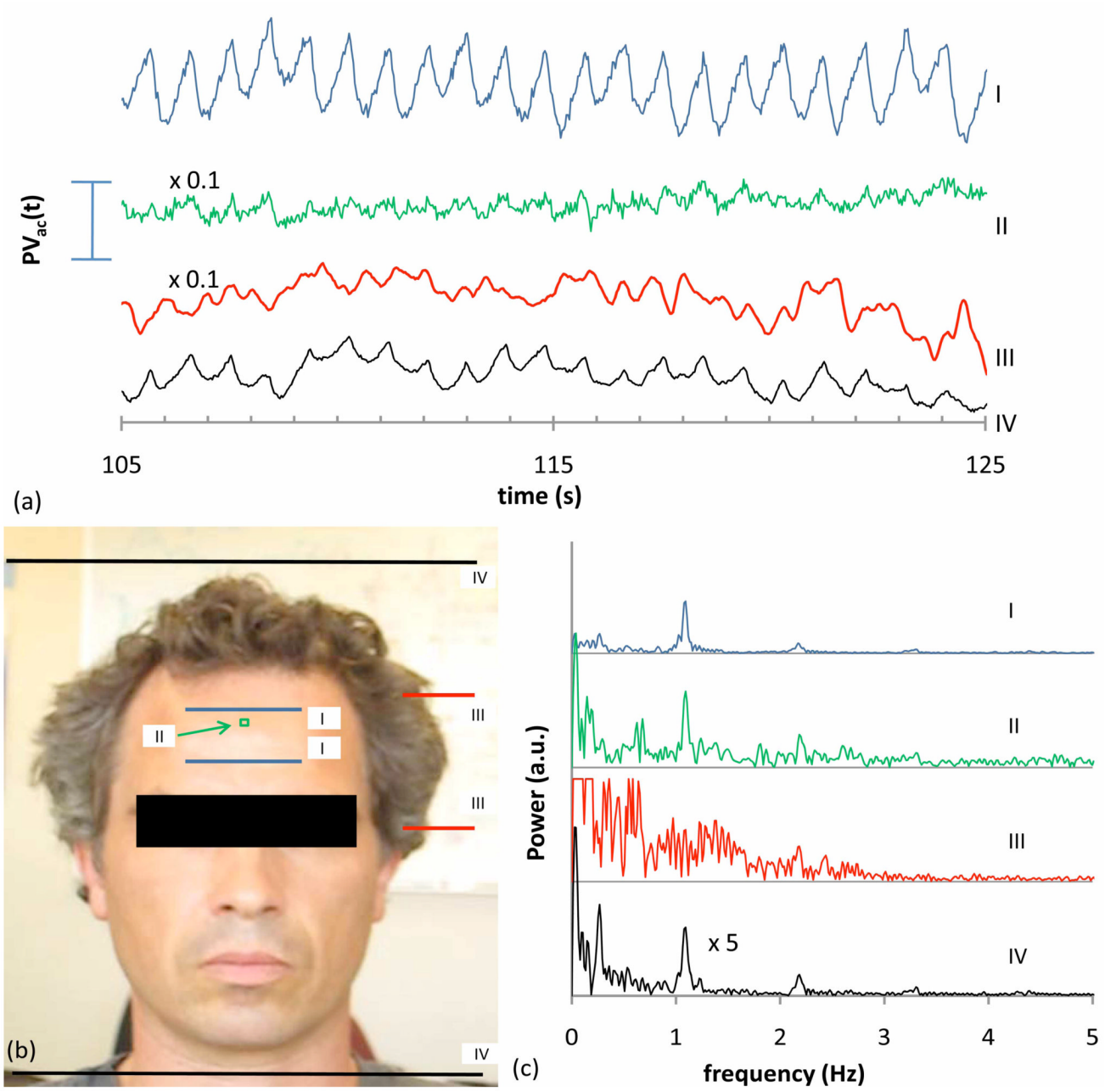


**Fig. 2.**

(a) $PV_{AC}(t)$ signals (G channel) for four ROI (I–IV) indicated in (b). (c) Corresponding power spectra. Signals for ROI's II and III are reduced (× 0.1) for clarity. The bar in (a) represents 10 pixel values for II and III and 1 for I and IV. The power spectrum for ROI IV is displayed ×5.

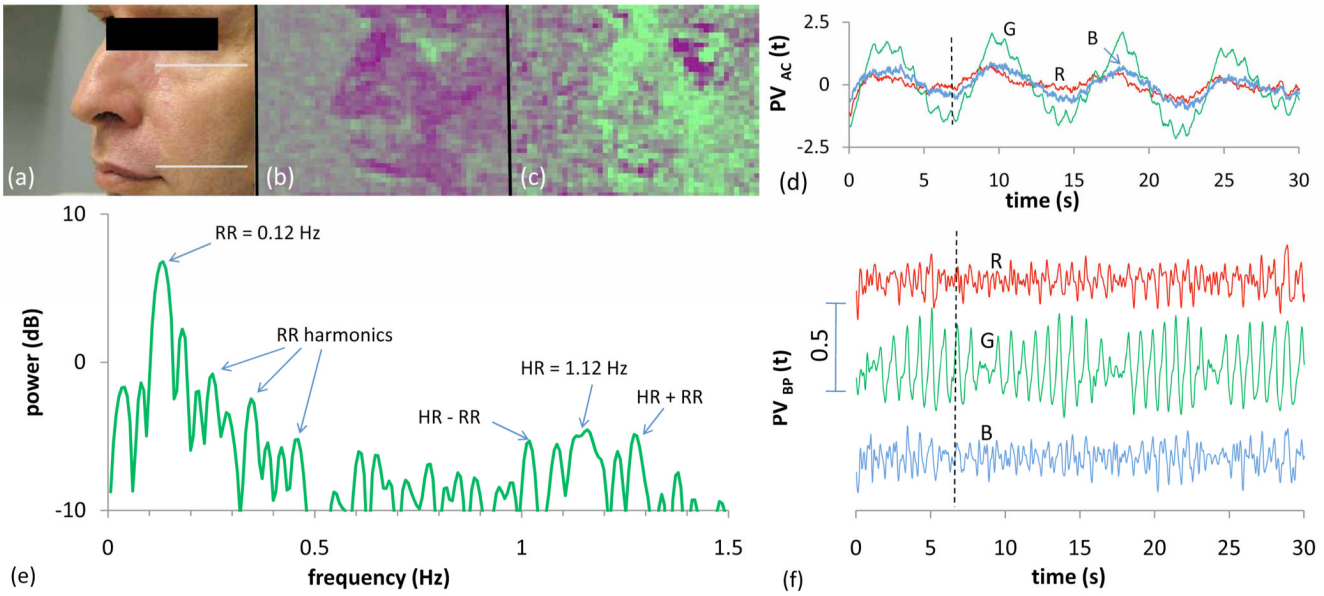


**Fig. 3.**

(a–c) A movie excerpt (frame 179, $t$ = 6 s, (Media1)), selected to demonstrate a low signal for $PV_{AC}(t)$, (b) and high signal for $PV_{BP}(t)$ (c). (d) $PV_{AC}$ ($t$) for the ROI indicated in (a), for the R, G and B channels, displayed up to $t$ = 30 s (media 1 shows up to $t$ = 15 s). (e) Power spectrum for the G channel indicating amplitude modulation of RR (≈ 0.12 Hz) and HR (≈ 1.12 Hz). (f) $PV_{BP}$ ($t$) signals, displaying an amplitude modulated HR signal for the G channel. Vertical dashed lines in (d) and (f) indicate the time of the movie excerpt.

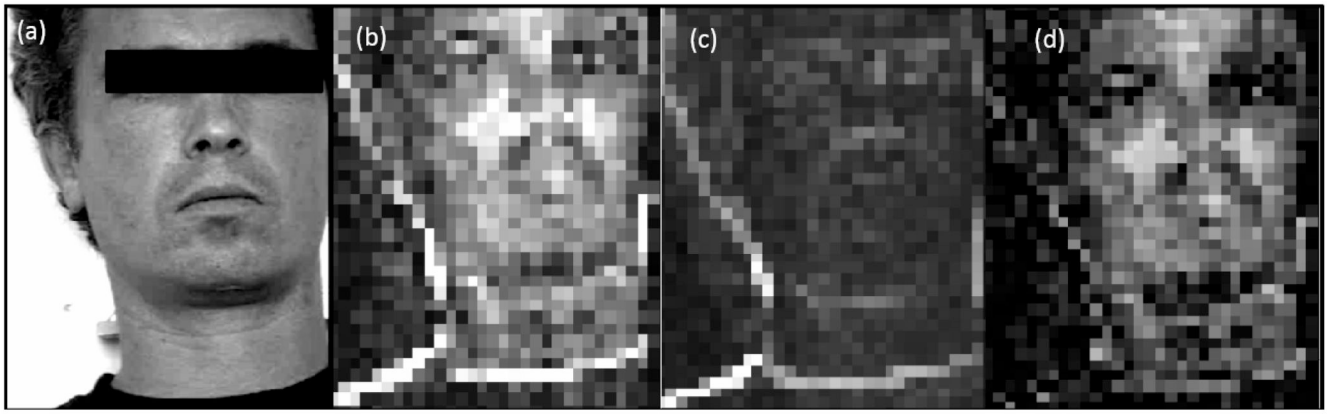


**Fig. 4.**
(a) Still (G channel only) from a movie. (b) Corresponding power map (at HR = 1.06 Hz) including artifactual high powers in areas with high contrast. (c) The movement artifact map consisting of average powers for bandwidths (0.80 – 0.95 and 1.17– 1.33 Hz). (d) Artifact corrected map: map (b) minus map (c).

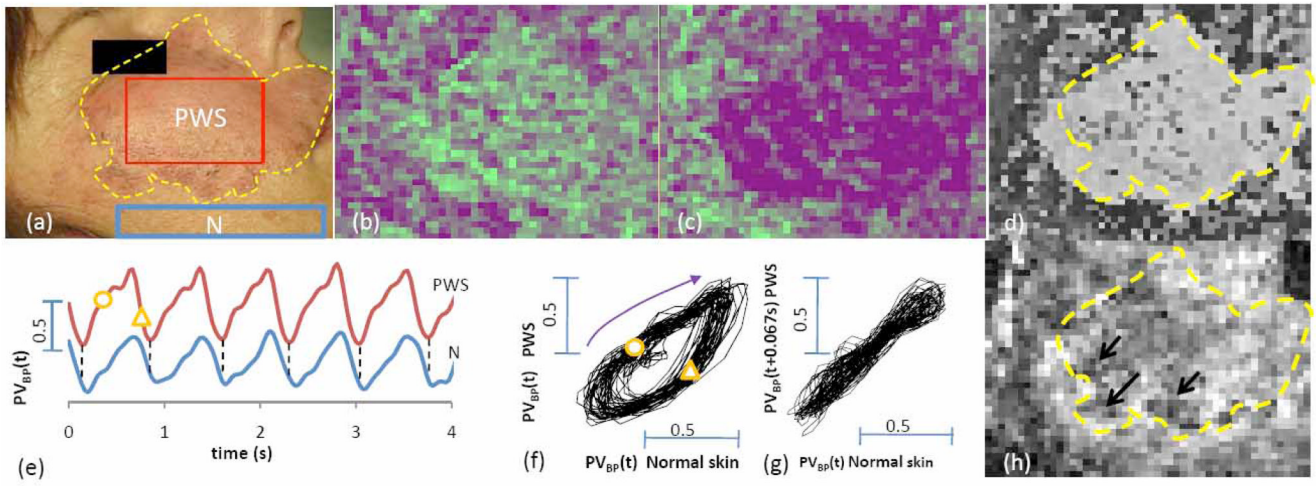


**Fig. 5.**

(a) Treated PWS area (dashed line) and 2 ROI (PWS and normal skin). (b–c) Frames 9 and 22, respectively, (Media 2). Intensities in (b–c) and Media 2 are linearly proportional to $PV_{BP}(t)$ (BP filter: 0.8 – 6 Hz). (d) Phase map (computed for 1.43 Hz) showing clear contrast between PWS and normal skin. (e) A fragment of the $PV_{BP}(t)$ signals in the ROI's, dashed lines indicate the lowest points for the PWS signal occurring prior to those for the normal skin signal. (f,g) Lissajous presentations of these signals. The circle and triangle in (e,f) indicate the phases for the images in (b) and (c), respectively. (h) Power map, arrows illustrate areas with relatively low pulsatility surrounded by areas with high pulsatility.

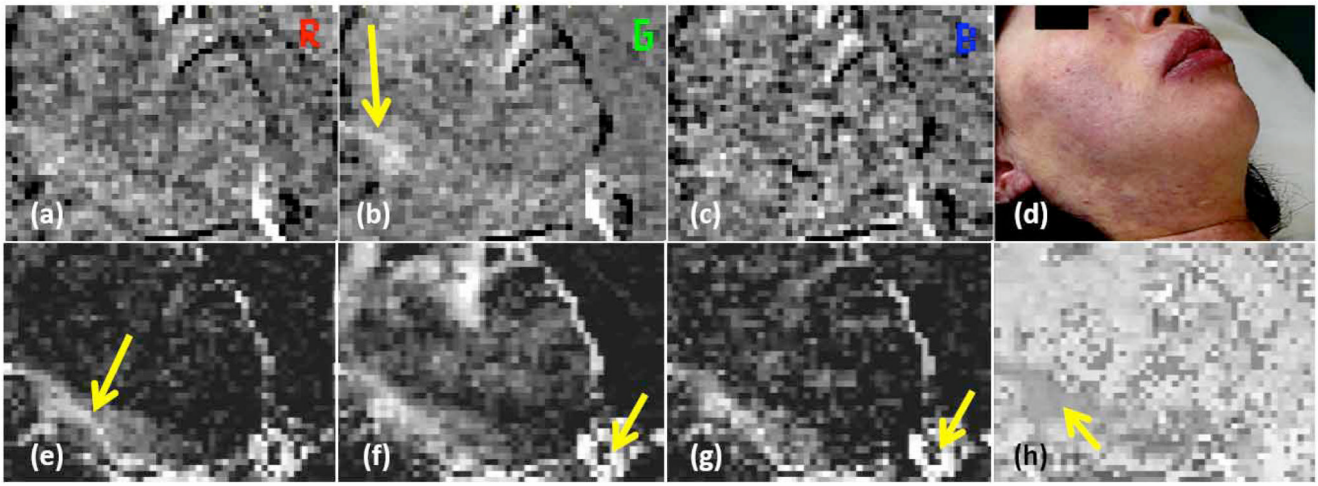


**Fig. 6.**

(a–c) $PV_{BP}(t)$ for R, G and B channels, respectively and (d) the original movie, a screenshot of (Media 3) ($t$ = 3.3 s.). (e–g) Corresponding power maps for R, G and B for the HR frequency (1.06 Hz) and the full 30 s. movie. Arrows in (b,e) indicate a structure which may be the right carotid artery. Arrows in (f,g) indicate displacement artifacts caused by the left carotid artery. (h) Phase map for the G channel, the arrow indicates a gradient of the phase.